Journal of Analytical and Applied Pyrolysis 109 (2014) 258–265

Contents lists available at ScienceDirect

Journal of Analytical and Applied Pyrolysis

journal homepage: www.elsevier.com/locate/jaap

An investigation on the texture and microstructure of carbonized charcoals produced by two-step pyrolysis

Khalid Elyounssi[a,b,*], Mohammed Halim[b]

[a] Centre de Recherche Forestière, Avenue Omar Ibn El Khattab, BP 763 Agdal, Rabat, Morocco
[b] Faculté des Sciences de Rabat, 4 Avenue Ibn Battouta, B.P. 1014 RP, Rabat, Morocco

ARTICLE INFO

Article history:
Received 3 March 2014
Accepted 13 June 2014
Available online 19 June 2014

Keywords:
Charcoal
Two-step pyrolysis
Texture
Microstructure
FTIR
XRD

ABSTRACT

In our previous work, we demonstrated a novel two-step pyrolysis method that increased the final char yield. The control of the final structure is another crucial issue in charcoal making. No structural study has yet been performed on charcoal produced by this two-step pyrolysis method. Here, we conducted two-step pyrolysis experiments (a pyrolysis step at 360 °C, followed by a carbonization step at 900 °C) on 102 cubes of eucalyptus wood samples. We selected carbonized charcoals (after two-step pyrolysis) that had different solid residue yields at the end of the first pyrolysis step to monitor the changes in their texture and structure using visual inspection, infrared spectroscopy (IR) and X-ray diffraction (XRD) analysis. Visual inspection showed different texture categories in terms of the carbonized charcoal defects, depending on their solid residue yield at the end of the first step: samples that were swollen and burst, samples that were split and samples that showed no abnormal defects. The IR spectra of the resulting carbonized charcoals showed no significant differences in their chemical structure. Conversely, their XRD patterns showed that the increase in char yield was accompanied by an increase in the formation of graphite crystallites. In particular, graphite crystallite formation was optimized for charcoals obtained by applying the second pyrolysis step when their solid residue yield was approximately 50% at the end of the first step. These findings open up new areas of exploration for in-depth studies to control the structure of charcoal.

1. Introduction

Currently, there is increasing interest in the use of charcoal from biomass for a variety of potential uses. Charcoal is used for energy [1–4], for the chemical reduction of ores such as iron and silicon in the metallurgical industry [5] and for adsorption purposes [6,7], but it has also been investigated for use as a soil amendment to improve the effect of fertilizer [8,9] and as a material for advanced applications (e.g., anodes for fuel cells) [10,11]. For such uses, the improvement of the char yield from biomass is a key question, but it is also crucial to control the texture and structure of the charcoal.

In our previous work [3,4], we tested a two-step pyrolysis method consisting of a low temperature step (low heating rate) followed by a rapid rise in the solid residue's charring temperature up to 900 °C (high heating rate), which increased the final char yield from eucalyptus wood (compared with the char yield obtained using one-step pyrolysis from ambient temperature to 900 °C, using the same wood). The extent of the increase in the final char yield from two-step pyrolysis was a function of the decomposition stage of the sample at the end of the first pyrolysis step, expressed by its solid residue yield. This increase was greatest when the second step (temperature increase to 900 °C) was applied to samples that had solid residue yields of approximately 50% at the end of the first step. The resulting char yield was comparable to that obtained using pyrolysis under moderate pressure (1 MPa) [2]. A legitimate question can be raised: Can charcoals produced by two-step pyrolysis present other desired properties (e.g., enhanced crystal structure) in addition to an increased yield?

It is known that carbonization of lignocellulosic feedstock at high temperatures can enhance the formation of graphite crystallite within the obtained charcoal [12–14]. Carbon materials containing a significant amount of graphite crystallite are prized for their considerable electrical conductivity, and they are produced by carbonization at temperatures exceeding 900 °C. Therefore, the two-step pyrolysis of wood samples would result in charcoals with enhanced graphite crystallite formation because it contains a

* Corresponding author at: Centre de Recherche Forestière, Avenue Omar Ibn El Khattab, BP 763 Agdal, Rabat, Morocco. Tel.: +212 537666405; fax: +212 537671151.
E-mail addresses: k.younssi71@gmail.com (K. Elyounssi), halim@fsr.ac.ma (M. Halim).

http://dx.doi.org/10.1016/j.jaap.2014.06.003
0165-2370/

carbonization step at 900 °C. However, it has yet to be determined whether the formation of graphite crystallite in charcoal can be optimized by applying the second pyrolysis step when the solid residue yield is approximately 50%, as the yield has been optimized. On the other hand, we noted during two-step pyrolysis experiments that the charcoals obtained with different increased yields also had different textures. Significant differences in shape and texture were observed, depending on the solid residue yield at the end of the first step. Since no textural or structural study has yet been carried out on charcoal produced by two-step pyrolysis, we decided to further examine this issue.

In this work, we investigated the changes in the texture and microstructure of carbonized charcoals obtained from two-step pyrolysis on eucalyptus wood samples relative to their solid residue yield at the end of the first pyrolysis step. Our objectives were to explore (1) whether the charcoals obtained with increased yields, especially that with a maximum increase in yield, also present an interesting chemical and crystal structure and (2) how the structural transitions of the samples at the end of the first step, as reflected mainly in their mechanical properties at the microstructural level, can affect the final texture of the two-step pyrolysis charcoals. First, we visually inspected all carbonized samples used in two-step pyrolysis to assess changes in texture. We then investigated the chemical structure and the microstructure of selected charcoal samples using infrared spectroscopy (IR) and X-ray diffraction (XRD) analysis, which are generally suited to this purpose [12–21,23,24]. Finally, we tried to explain the correlation between the final texture of the carbonized samples and their microstructure before the carbonization step (at 900 °C).

2. Materials and methods

2.1. Plant material

Samples of eucalyptus wood (*Eucalyptus grandis*) from Morocco were used as whole biomass. All the wood samples were taken from a debarked trunk and were sawn in 2-cm cubes. Prior to pyrolysis, they were dried at a temperature of 103 °C for 48 h in a "Memmert ULE 700" electric oven and weighed to determine their dry mass. Eucalyptus wood was used in this work because of its widespread use as a feedstock for bioenergy applications and because it is considered to yield a good quality of charcoal. In total, 102 wood samples were used in the pyrolysis experiments, which is an adequate sample size to produce reliable results.

2.2. Pyrolysis experiments

The two-step pyrolysis experiments were carried out in a "Carbolite" isothermal electric furnace. Woody samples were each placed in a covered but unsealed 25-mL nickel crucible to protect them from the oxidizing atmosphere. The nascent volatiles produced during pyrolysis could escape easily, allowing the pressure in the sample environment to remain practically equal to the ambient value.

Two-step pyrolysis consisted of a first isothermal pyrolysis step at a low temperature of 360 °C, followed by a second carbonization step at a high temperature of 900 °C. Different two-step pyrolysis runs were carried out. In each run, the second step was applied when the solid residue yield obtained at the end of the first step at 360 °C (called $Y1$ and defined by Eq. (1)) had a certain value. Different times were adopted in order to yield different values of $Y1$ after the first pyrolysis step. For each fixed time, three samples were placed simultaneously in the furnace, which had been heated previously to a temperature of 360 °C. The samples were cooled down (first in the oven at 103 °C and then in a desiccator) and weighed. The $Y1$ value was determined for each of the three samples and their mean was calculated. The three samples within the covered crucibles were then placed in the oven at a temperature of 900 °C (i.e., the carbonization step) using a stainless steel support for a duration of 10 min. The yield of the carbonized solid residue obtained from two-step pyrolysis (called $Y2$ and defined by Eq. (2)) was then determined for each of the three samples. We must note here that the temperature of the oven dropped to approximately 800 °C when the stainless steel support and crucibles were inserted, and it took approximately 5 min to reach the temperature of 900 °C again.

$Y1$ and $Y2$ are defined by Eqs. (1) and (2), respectively, where M_{c1}, M_{c2} and M_w are the dry masses of the pyrolyzed solid residue, the carbonized solid residue and the wood sample, respectively.

$$Y1 = \frac{M_{c1}}{M_w} \times 100 \tag{1}$$

$$Y2 = \frac{M_{c2}}{M_w} \times 100 \tag{2}$$

In the following discussion, the solid residues obtained at the end of the first step at 360 °C will be referred to as pyrolyzed samples, while those obtained from two-step pyrolysis (after the step at 900 °C) will be referred to as carbonized samples. For clarity, a single pyrolyzed (or carbonized) sample will be referred to as PX (or CX, respectively), where X is its corresponding $Y1$ value.

2.3. Visual inspection

All of the pyrolyzed and carbonized samples (i.e., samples before and after undergoing the second pyrolysis step) were examined visually to detect altered physical features or defects (cracks, swelling, split, etc.). The objective was to assess the changes in texture of the carbonized samples that occurred during the second pyrolysis step at 900 °C and to relate these features to those of the pyrolyzed solid residues at the end of the first pyrolysis step.

2.4. Sample selection

To monitor the changes in structure using IR and XRD analysis, we selected pyrolyzed solid residues obtained with $Y1$ values ranging from the minimal experimental value of 29.1% (corresponding to a sample pyrolyzed at 360 °C for 360 min) to 100% (corresponding to wood). To this end, we adopted samples P30, P40, P50, P60, P70, P80 and P100, corresponding to experimental $Y1$ values approximately equal to 30%, 40%, 50%, 60%, 70%, 80% and 100% (the measured values were 29.1%, 40.0%, 49.0%, 61.6%, 71.6% and 80.7%). We retrieved a portion of each pyrolyzed sample for IR and XRD analysis and carried out the carbonization step at 900 °C on the remaining sample portion. Carbonized samples were then obtained: namely C30, C40, C50, C60, C70, C80 and C100, which were, in turn, analyzed using IR and XRD.

2.5. FT-IR spectroscopy

Fourier transform infrared spectrometry analysis (FT-IR) was carried out using the KBr pellet technique with a VERTEX 70 FT-IR spectrometer equipped with a 24-bit data acquisition system based on delta-sigma ADCs and a DigiTect^{TM} detector. KBr pellets were prepared by grinding 1 mg of dry charcoal sample with 100 mg of dried KBr. The spectrum range covered was 400–4000 cm^{-1}.

2.6. X-ray diffraction

Powder XRD measurements of the selected pyrolyzed and carbonized samples were conducted using a pan analytical X'pert Pro

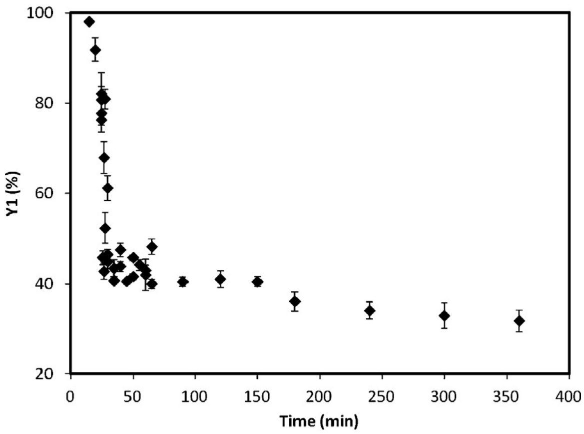

Fig. 1. Changes in solid residue yields at the end of the first pyrolysis step at 360 °C as a function of time (calculated on dry basis). Error bars show the standard deviation.

instrument equipped with a Cu anode as a Cu-Kα radiation source (λ = 1.544 Å). The charcoal samples were milled to pass through a 250-μm sieve (60 mesh). The X-ray generator was set to 45 kV and 40 mA, and the XRD patterns were recorded by step scanning over the 3–90° range of 2θ. The step size was 0.06°, and the scan step time was 121 s. The XRD patterns were subjected to background correction to determine the (0 0 2) and (1 0 0) peak positions and their respective full width at half maximum (FWHM). The Debye–Scherer equation was used to calculate the crystallite size.

3. Results and discussion

3.1. Changes in char yield

Fig. 1 shows the changes in the pyrolyzed solid residue yields ($Y1$) obtained at the end of the first pyrolysis step at 360 °C as a function of time. This first step is simply an isothermal pyrolysis at 360 °C; the shape of the curve was similar to typical plots characteristic of the pyrolysis of lignocellulosic materials. As the pyrolysis time increased, a first dramatic mass loss was observed, corresponding mainly to the decomposition of hemicelluloses and cellulose. From the time the $Y1$ value reached approximately 50%, the mass loss became much smaller, corresponding mainly to the decomposition of the remaining lignin.

Fig. 2 shows the changes in the carbonized sample yield ($Y2$) vs. the pyrolyzed solid residue yield ($Y1$). It is apparent from this figure that the values of $Y2$ depended strongly on those of $Y1$. For

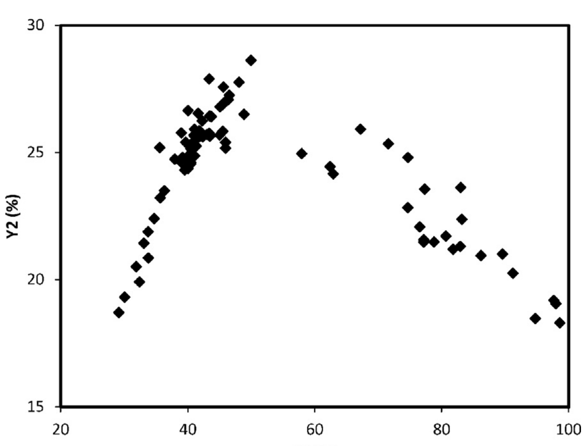

Fig. 2. Changes in char yield from two-step pyrolysis vs. the solid residue yield at the end of the first pyrolysis step (calculated on dry basis).

the wood sample (i.e., $Y1$ value equal to 100%), the carbonized sample had a $Y2$ value of only 18.0%. This result is typical of the flash pyrolysis of wood at a temperature of approximately 900 °C, which generally results in char yields in the 15–20% range [25]. As the first pyrolysis step at 360 °C advanced and the $Y1$ value decreased, the corresponding $Y2$ value increased until it reached a maximum of 28.6%, obtained at a $Y1$ value of 49.9%. In addition, as the $Y1$ value dropped below 50%, the corresponding $Y2$ value began to decrease. This corroborates the results we reported earlier [3,4], in which we recommended that lignocellulosic feedstock should first undergo a low-temperature pyrolysis (e.g., at 360 °C) until the $Y1$ value is approximately 50% (when almost all the hemicelluloses and cellulose are completely decomposed) before undergoing a second pyrolysis step at 900 °C to optimize the final char yield from two-step pyrolysis.

3.2. Changes in texture

The pyrolyzed solid residues obtained from the first pyrolysis step did not show unusual features. As the pyrolysis time increased, the solid residues shrank and showed some cracks, more closely approaching the texture of charcoal. This behavior is as expected since the first step is a simple isothermal pyrolysis. In particular, the resulting solid residue had a yield of only 29.1% for a pyrolysis time of 360 min and can be considered as conventional charcoal (charcoal produced in kilns using simple pyrolysis).

Conversely, a visual inspection of the carbonized samples obtained from two-step pyrolysis showed that there were three main texture categories, depending on the solid residue yield value ($Y1$) at which the second pyrolysis step at 900 °C was applied to the pyrolyzed samples. This categorization included (i) samples that were swollen and burst ($48.8 \leq Y1 \leq 98.6\%$); (ii) samples that were split into two pieces ($40.4 \leq Y1 \leq 46.6$); and (iii) samples that had no abnormal defects except some superficial cracks ($40.0\% \leq Y1 \leq 29.1\%$). Fig. 3 shows images of some samples representative of each category (see supplementary materials for more details).

All carbonized samples obtained from two-step pyrolysis including a first pyrolysis step at 360 °C with an $Y1$ value higher than approximately 50% were apparently swollen and burst (category i). The bursting of the samples during carbonization at 900 °C was greatest when the $Y1$ values were in the 61.6–83.1% range. These carbonized samples showed several breaks parallel to the longitudinal direction of the wood. Each sample appeared to be split up into several pieces (typically four), which were, however, still connected to form one sample. This bursting could be attributed to the quick release and escape of volatiles during the second pyrolysis step at 900 °C. Indeed, pyrolyzed samples with $Y1$ values within the 61.6–83.1% range still contained hemicelluloses and cellulose that were not completely decomposed. These two constituents decomposed very rapidly at 900 °C and released a high amount of volatiles (between 64.2% and 73.1% of the pyrolyzed sample's initial mass) during a short time, inducing a pressure increase within the samples and causing bursting. The bursting was less significant for the carbonized samples with corresponding $Y1$ values in the 48.8–58% range, very likely because the amounts of the volatiles released during carbonization at 900 °C were smaller (between 48.9% and 59.0% of the pyrolyzed sample's initial mass).

Surprisingly, we noted that pyrolyzed samples with $Y1$ values higher than 86.1% did not show significant swelling or bursting. Theoretically, these samples must have released more volatiles during carbonization at 900 °C than the other samples within category (i) because almost none of the constituents (especially cellulose and hemicelluloses) were decomposed at the end of the first pyrolysis step at 360 °C. As a result, they should have suffered more significant bursting. However, we observed only one break in the

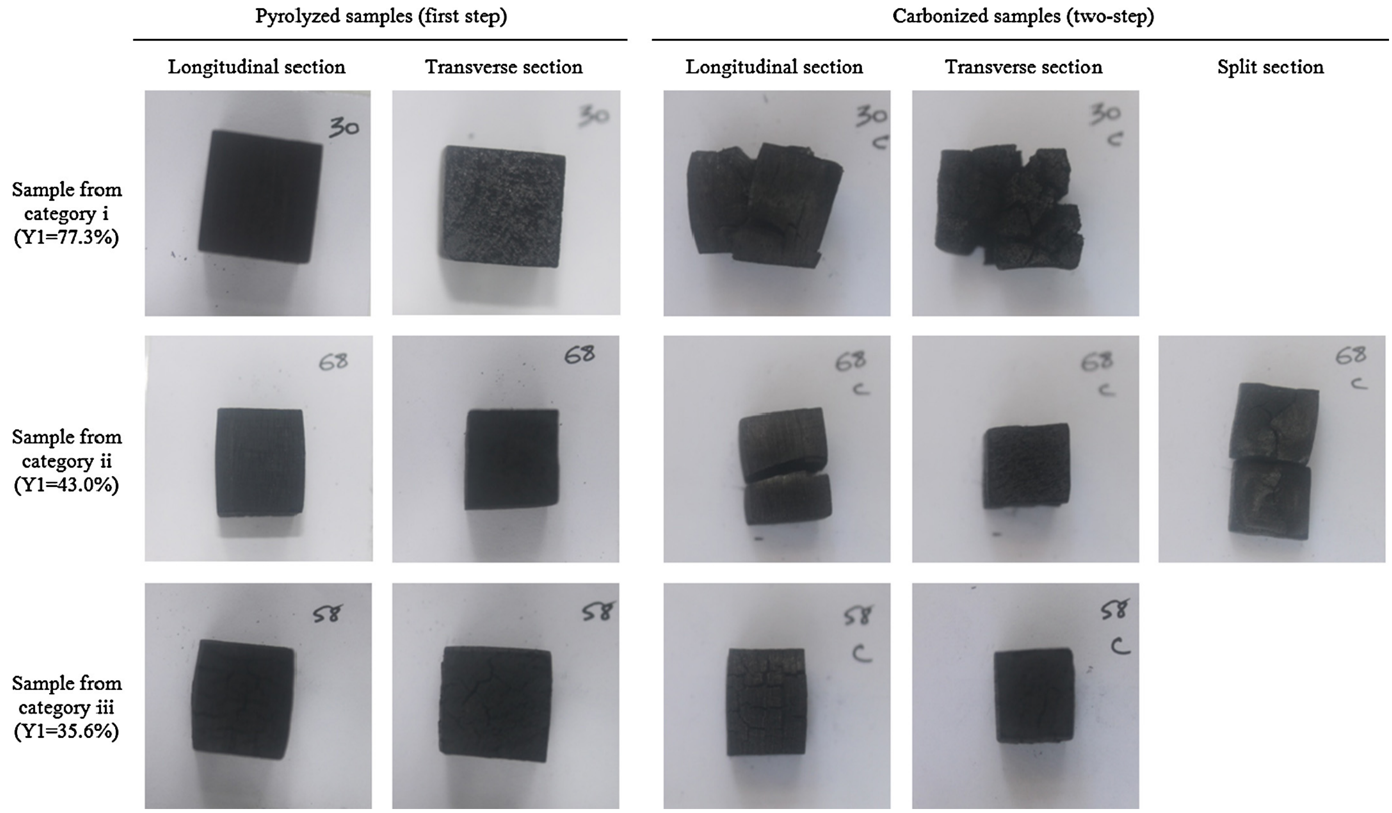

Fig. 3. Images of samples representative of each category in terms of texture defects.

longitudinal direction in these samples, accompanied sometimes by another break in the transverse direction. We conclude from this observation that the volatiles released during the pyrolysis step at 900 °C cannot independently explain the occurrence of swelling or bursting. A complementary explanation could be sought in the initial microstructure of the pyrolyzed solid residues before the carbonization step at 900 °C (see Section 3.5).

Unlike samples within the previous category, the carbonized samples obtained from two-step pyrolysis including a first pyrolysis step with a *Y*1 value in the 40.4–46.6% range (no measured values of *Y*1 between 46.6% and 48.8% were obtained in this work) were split into two pieces following an approximately planar split section, perpendicular to the longitudinal direction of the wood (category ii). Except for the observed splits, these samples preserved their initial cubic shape relatively well, and their outer surfaces were quite smooth. The escape of volatiles from within the samples in this category during the carbonization step at 900 °C seemed not to be strong enough to cause any significant swelling or bursting. The amounts of these volatiles (between 37.7% and 41.5% of the pyrolyzed sample's initial mass) were, in fact, lower than those released by the samples of category (i). However, again, the relationship between the initial microstructure of the pyrolyzed samples before the carbonization step at 900 °C and the nature of the observed defects (split) remains to be confirmed (see Section 3.5).

Finally, no remarkable defects were observed in carbonized samples that underwent a first pyrolysis step until reaching an *Y*1 value in the 29.1–40.0% range (category iii). The cubic shape of the samples was preserved, and there were only small superficial cracks, which had been present in the pyrolyzed samples before the carbonization step at 900 °C. The small amounts of volatiles released by the samples at 900 °C (between 35.7% and 40.2% of the pyrolyzed sample's initial mass) did not affect the texture of the samples' carbonaceous matrices. To our knowledge, no similar partitioning of the texture of carbonized charcoal has been previously reported. Charcoals within the different categories need to be characterized in terms of their physical and chemical properties in order to draw relevant conclusions with respect to their potential use.

3.3. Assessment of chemical changes using FT-IR

We remind the reader that our objective was first to investigate the structure of the carbonized charcoals resulting from two-step pyrolysis. However, we also investigated the structure of the pyrolyzed solid residues after the first pyrolysis step to explore how this step may condition the final two-step charcoal structure. Fig. 4(a) shows the changes in the FT-IR spectra of the pyrolyzed solid residues obtained with different yields (i.e., P30, P40, P50, P60, P70 and P80 samples), as well as the FT-IR spectrum of the wood sample. The FT-IR spectrum of our wood sample showed typical bands specific to raw lignocellulosic materials. A list of the main vibrations displayed in this spectrum and their functional group assignments are shown in Table 1.

We can see from Fig. 4(a) that, until the decomposition stage corresponding to an *Y*1 value of 60%, the charring samples indeed underwent chemical transformations, but the chemical structure of the native wood sample was still coherent. All the absorption peaks present in the FT-IR spectrum of the wood sample were still present in the FT-IR spectra of the P80, P70 and P60 samples, although with decreasing intensities (except for the 1700 cm^{-1} and the 1600 cm^{-1} bands, corresponding, respectively, to the C=O and C=C stretching vibrations [15–20], which showed slight increases for the P60 sample). Dehydration and the partial degradation of holocelluloses were the main chemical transformations and were mainly expressed by decreases in peak intensities in the 3600–3000 cm^{-1} and 1030–1160 cm^{-1} ranges, corresponding to the O—H and C—O stretching vibrations, respectively [15–20]. In particular, cellulose,

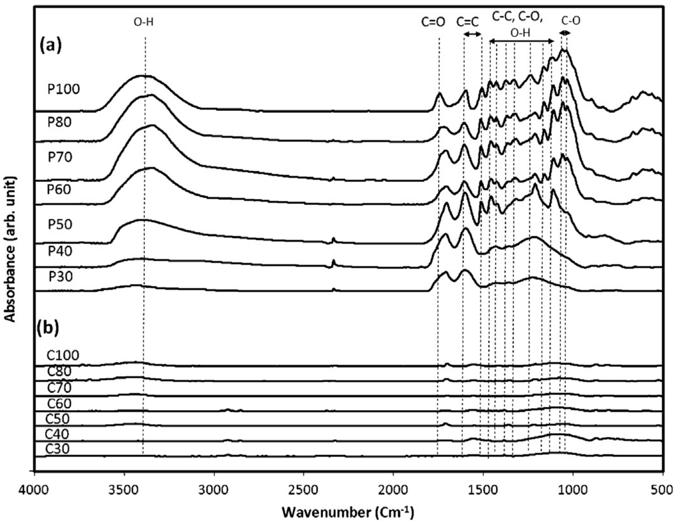

Fig. 4. Stacked FT-IR spectra of (a) pyrolyzed solid residues obtained from the first pyrolysis step with yield values ranging from 100% (raw wood) to 30%, and (b) carbonized samples obtained by applying the second pyrolysis step to solid residues described in (a).

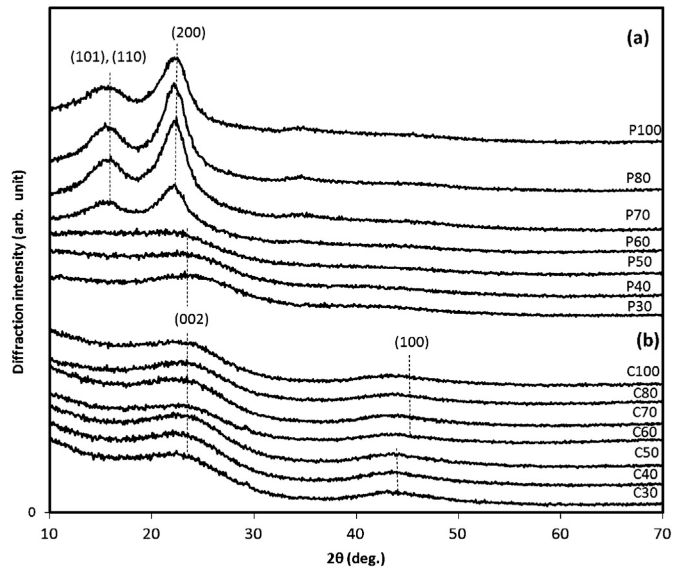

Fig. 5. Stacked X-ray diffraction patterns of (a) pyrolyzed solid residues obtained from the first pyrolysis step with yield values ranging from 100% (raw wood) to 30%, and (b) carbonized samples obtained by applying the second pyrolysis step to solid residues described in (a).

although partially decomposed for the P80, P70 and P60 samples, was still present, as confirmed by its indicative bands at 1030 cm^{-1} and 1060 cm^{-1} (C—OH vibration) [15,17,18] and at 1160 cm^{-1} (C—O—C ether vibration) [15–17,19].

The FT-IR spectrum of the P50 sample showed the first significant change, in the sense that the bands indicative of cellulose, and a priori hemicelluloses, had vanished (i.e., the 1030 cm^{-1} and the 1060 cm^{-1} bands dramatically decreased, and the 1160 cm^{-1} band practically disappeared), confirming that these two constituents were almost completely decomposed. This FT-IR spectrum was characterized by stronger C═C and C═O stretching vibration bands at 1600–1500 cm^{-1} and 1700 cm^{-1}, respectively, which are indicative of aromatic enrichment and products formed from lignin decomposition [18]. These latter products were also reflected by vibrations characteristic of lignin components, such as the C—O stretching vibration of phenolic compounds observed at 1212 cm^{-1} [15,16,18,20].

As the pyrolysis process advanced and the $Y1$ value decreased (P40 and P30 samples), the O—H stretching vibration at 3600–3000 cm^{-1} continued to lose intensity. The C═O and C═C stretching vibrations slightly decreased but, along with the stretching vibration of the aromatic C—H vibration at 3140 cm^{-1} [18,21], became more important relative to the other peaks, which is indicative of more prominent aromatic component formation. To summarize, we can see from Fig. 4(a) that there were three distinct categories of spectra: the first corresponding to the P80, P70 and P60 samples, as well as the wood sample ($Y1 > 50\%$); the second to the P50 sample; and the third to the P40 and P30 samples ($30\% \leq Y1 \leq 40\%$). This categorization is in agreement with that described in Section 3.2, which was elaborated based on a visual inspection of the carbonized samples.

Table 1
Assignment of the main characteristic vibrations of the wood sample's FT-IR spectrum.

Wavenumber (cm^{-1})	Characteristic vibrations
3403	O—H stretching of H-bonded hydroxyl
1741	C═O stretching of carboxyl and carbonyl groups
1596	C═C stretching of aromatic ring
1506	C═C stretching of aromatic ring
1461	C—H bending of CH3 (asymmetric) and CH2-groups
1426	O—H bending
1372	C—H bending of CH3 (symmetric) groups
1330	C—H bending of CH groups
1235	C—O stretching of aryl alkyl-ether and phenol
1160	C—O stretching of pyranose ring
1113	C—H bending of syringyl and gaiacyl units
1036–1059	C—O stretching of C—OH groups

On the other hand, Fig. 4(b) shows the FT-IR spectra of the carbonized samples. The peak intensities of these spectra were much lower compared to those of the pyrolyzed samples (up to 3 orders of magnitude). All the carbon functionalities had practically vanished after the carbonization of the samples at 900 °C. Furthermore, all the FT-IR spectra of the carbonized samples were similar. That is, the peak intensity of a given carbon functionality had approximately the same magnitude across the different FT-IR spectra. We conclude that there were no significant differences in chemical structure among the carbonized charcoals. In particular, the FT-IR spectrum of the C50 sample was similar to the FT-IR spectra of the other carbonized samples, showing that the maximum increase in char yield ($Y2$) obtained for this sample was not associated with particular carbon functionalities. The disappearance of these carbon functionalities seems to occur subsequently to the interactions at 900 °C responsible for the char yield increase (discussed elsewhere [4]).

3.4. Assessment of microstructural changes using XRD

Fig. 5(a) shows the XRD patterns of the pyrolyzed solid residues obtained at different yields. The XRD pattern of the P100 sample (wood) shows two main peaks, which are attributed to the reflections of crystalline cellulose present in wood: the first at $2\theta = 22.2°$, corresponding to the (2 0 0) plan, and the second at $2\theta = 15.6$, which is known to be a composite of two peaks corresponding to the (1 0 1) and (1 1 0) plans [12,18,20,22]. As seen in Fig. 5(a), these two peaks were also present in the XRD patterns of the P80, P70 and P60 samples, indicating that crystalline cellulose was still present until the decomposition stage corresponding to $Y1 = 60\%$. However, they became less intense and broader in the P60 XRD pattern, indicating the ongoing decomposition of cellulose within the charring residue. As the $Y1$ value continued to decrease, the peaks corresponding to crystalline cellulose vanished, which means that all the crystallinity of cellulose was lost (i.e., almost all the cellulose

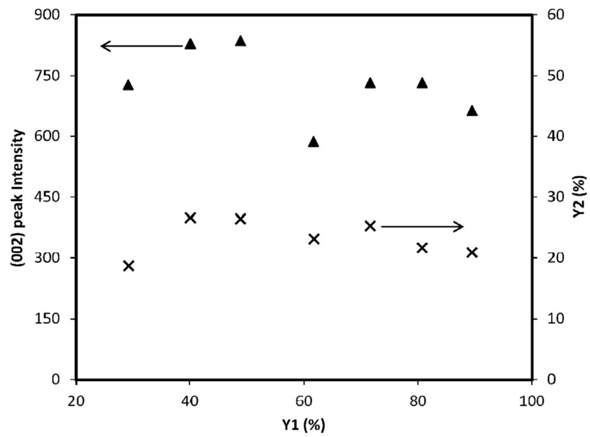

Fig. 6. Changes in the char yield ($Y2$) of the selected carbonized samples (lower curve) and the (0 0 2) peak intensity of their XRD patterns (upper curve). Note: the (0 0 2) and (1 0 0) peak intensities of the C60 XRD pattern seem to be outstanding values.

originally present in the wood had completely decomposed). In particular, the XRD pattern of the P50 sample was remarkably flat, showing the amorphous structure of this sample, although a new peak started to appear at approximately $2\theta = 22.3°$. This result is in excellent agreement with the results of the FT-IR analysis discussed in Section 3.3. The decomposition stage corresponding to $Y1 = 50\%$ seems to be the beginning of a turning point in the pyrolysis process. Peaks at $2\theta = 23.2$ and $2\theta = 23.9$ were, however, more obvious in the XRD patterns of the P40 and P30 samples, respectively. Peaks at such 2θ values for carbon materials are attributed to the (0 0 2) plan reflection of the graphite crystallites and are indicative, here, of the progressive stacking of graphene sheets within our samples, the structure of which approached that of turbostratic carbon [12,18].

On the other hand, all the XRD patterns of the carbonized samples shown in Fig. 5(b) had the same shape, similar to that of turbostratic carbon [12,18,23]. Peaks corresponding to the (0 0 2) reflection were observed at 2θ values in the 22.9–23.2 °C range. Table 2 shows the results of the microstructure analysis of both the carbonized samples and the pyrolyzed samples P50, P40 and P30. All the (0 0 2) peaks had comparable FWHMs. In all the samples shown in Table 2, the graphite crystallites were composed of approximately three graphene sheets. Similar graphite crystallite sizes were also reported by Paris et al. and Smith et al. [12,24]. However, these (0 0 2) peaks had variable intensities. Note that the XRD patterns of the carbonized samples had (0 0 2) peak intensities that were much higher than those observed for the P50, P40 and P30 samples. This is expected, as the carbonization of woody material at high temperatures is known to enhance graphite crystallite formation. Fig. 6 shows changes in the char yield ($Y2$) of the selected carbonized samples and the (0 0 2) peak intensity of their XRD patterns. From this figure, it appears that there was a clear positive correlation between the two parameters displayed. The higher the (0 0 2) peak intensity was, the greater the $Y2$ value was. In a related paper, Kercher and Nagle [13] reported that, when the FWHM did not change (which is the case here), the increase in (0 0 2) peak intensity was attributed to an increased amount of turbostratic carbon. We can conclude then that the increased char yield during the second pyrolysis step at 900 °C was indeed accompanied by the formation of an increased amount of graphite crystallites and vice versa.

The XRD pattern of the C50 sample showed the highest (0 0 2) peak intensity, followed closely by that of the C40 sample. The C50 and C40 char yield values ($Y2$ values) were also the highest values obtained in this work from two-step pyrolysis. Moreover, the XRD pattern of the C50 sample showed the highest possible (0 0 2) peak intensity for carbonized charcoal in the given conditions (i.e., pyrolysis step at 900 °C for 10 min). The pyrolysis step at 900 °C was applied here to solid residues with a range of initial yields: from wood (P100) to well-charred sample (P30). Of all these possibilities, the C50 produced the highest (0 0 2) peak intensity and therefore contained the highest amount of graphite crystallites. This pyrolysis step (900 °C for 10 min) could be applied to the P30 sample (well-charred sample) rather than the P50 sample in order to produce charcoal with the highest amount of graphite crystallites. Our results showed that the C30 sample thus obtained not only had an $Y2$ value smaller than that of the C50 sample but also contained fewer graphite crystallites. Carbon materials with a significant amount of graphite crystallites are prized for their considerable electrical conductivity. Such materials are obtained by carbonizing, inter alia, woody materials at high temperatures (e.g., 900 °C). According to our results, the carbonization of pyrolyzed wood samples at high temperatures when their solid residue yield is approximately 50% appeared to be a key condition to optimize graphite crystallite formation. This result holds promise for developing charcoals with potential use as electricity conductors. Here again, no previous studies in the field have reported such observations: i.e., (1) that there is a positive correlation between the increase in char yield and the formation of graphite crystallite in charcoals resulting from two-step pyrolysis; and (2) an optimized increase in graphite crystallite formation in carbonized samples occurs when applying a second pyrolysis step to pyrolyzed solid residues with a yield of approximately 50% at the end of the first pyrolysis step.

3.5. Changes in texture vs. changes in microstructure

As discussed in Section 3.2, the amount of volatiles released by the samples during the carbonization step at 900 °C could explain why the observed defects occurred, but not why these defects included swelling, bursting or split. This suggests that the nature of these defects depended not only on the amount of the volatiles released but also on the microstructure of the samples being carbonized. According to the discussion in Sections 3.2–3.4, the pyrolyzed samples within a given category (i, ii or iii) had similar chemical and microstructural properties, as shown by the FT-IR and XRD analysis, which most likely resulted in the similar nature of their defects obtained during pyrolysis at 900 °C.

For instance, pyrolyzed samples obtained with $Y1$ values higher than 86.1% underwent minimal decomposition and had microstructures that were still similar to that of the initial wood. At this stage of decomposition, the chemical bonds between the three wood constituents (cellulose, hemicelluloses and lignin), which are responsible for mechanical properties such as strength and elasticity, were almost completely preserved. This seemed to prevent significant bursting caused by the volatiles released from within the sample.

Conversely, the microstructure of the pyrolyzed samples obtained with $Y1$ values in the 61.6–83.1% range was different. The wood constituents (hemicelluloses and, to a less extent, cellulose) underwent additional decomposition, causing the microstructure of the samples to undergo additional changes as well. In particular, hemicelluloses had very likely completely decomposed, and the bonds between the microfibrils within the cell wall were weakened. However, it can be assumed that the anisotropic mechanical properties, which are characteristic of the initial wood structure [12,26,27], were consistent for those samples. Indeed, measurements of mechanical properties carried out at the cell wall level using the nanoindentation technique [26] revealed that the Young's modulus of pyrolyzed wood samples in the axial direction was higher than those in the radial or tangential directions up to a pyrolysis temperature of 275 °C (this temperature very likely

Table 2
Results of the XRD analysis of the carbonized samples and three of the pyrolyzed samples.

Sample	Peak (0 0 2)						Peak (1 0 0)			
	2θ[a] (deg.)	FWHM[b] (deg.)	Lc[c] (Å)	d0 0 2[d] (Å)	N[e]	I[f]	2θ (deg.)	FWHM (deg.)	La[g] (Å)	I
C100	23.0	8.0	10.1	3.87	2.6	664	45.0	10.7	16.4	275
C80	23.1	8.3	9.7	3.84	2.5	733	44.4	9.0	19.6	265
C70	23.1	7.9	10.3	3.85	2.7	733	44.8	9.6	18.2	296
C60	23.2	8.1	10.1	3.83	2.6	588	44.6	9.5	18.5	253
C50	23.2	7.9	10.2	3.83	2.7	836	45.1	10.7	16.5	352
C40	22.9	8.3	9.8	3.88	2.5	829	44.9	9.8	17.9	339
C30	23.0	8.1	10.0	3.87	2.6	729	45.0	10.1	17.5	321
P50	22.3	7.8	10.4	3.99	2.6	497	43.8	9.7	18.0	88
P40	23.2	8.8	9.3	3.83	2.4	524	43.5	8.9	19.6	77
P30	23.9	8.8	9.3	3.72	2.5	580	43.4	8.5	20.7	98

[a] 2θ: peak position.
[b] FWHM: full width at the half-maximum.
[c] Lc: crystallite size in stacking direction.
[d] d0 0 2: distance between graphene sheets.
[e] N: number of graphene sheets.
[f] I: peak intensity after background subtraction.
[g] La: crystallite size in-plane. Note: the 0 0 2 and the 1 0 0 peak intensities of the C60 XRD pattern seem to be outstanding values.

corresponded to $Y1$ values in our 61.6–83.1% range, as the authors reported a 60% mass loss at a temperature of 325 °C). This may explain why, when carbonized at 900 °C, the high amount of volatiles released tended to burst the carbonaceous matrix along the weak direction (tangential or radial) rather than the strong direction (longitudinal).

In the same way, the microstructure of the pyrolyzed samples obtained with $Y1$ values in the 40.0–46.6% range substantially changed. The microstructure of wood was lost, as confirmed by IR and XRD measurements, and an amorphous structure developed. The isotropy of the mechanical properties of pyrolyzed wood has also been reported by Brandt et al. [26]. Moreover, the Young's modulus in the axial direction was slightly smaller than those in the radial and the tangential directions [26]. This may explain the propensity of split to occur following the new weak direction (the transverse direction), dividing the carbonized samples into two pieces.

4. Conclusions

In this study, we demonstrated the existence of three distinct categories of charcoals obtained by two-step pyrolysis in terms of their textural defects, which varied depending on their solid residue yield at the end of the first step: (i) samples that were swollen and burst; (ii) samples that were split into two pieces; and (iii) samples that showed no abnormal defects. Infrared spectroscopy and X-ray diffraction were used to investigate the chemical and crystal structure of charcoals within the different categories. In particular, our main finding was that the charcoal obtained by two-step pyrolysis in which the second pyrolysis step at 900 °C was applied when the solid residue yield at the end of the first step was approximately 50% showed the greatest increase in both yield and graphite crystallite formation. This charcoal holds promise for potential use in developing electricity conductors from carbon materials (e.g., fuel cell anodes). Measurements of other mechanical and physical properties (e.g., strength, surface area) for charcoals within the different categories were not in the scope of this study, and should be addressed in future research in order to draw more relevant conclusions with respect to the potential use of such charcoals in other applications (reduction of ores, adsorption, etc.)

Appendix A. Supplementary data

Supplementary data associated with this article can be found, in the online version, at http://dx.doi.org/10.1016/j.jaap.2014.06.003.

References

[1] M.J. Antal, W.S.L. Mok, G. Varhegyi, T. Szekely, Review of methods for improving the yield of charcoal from biomass, Energy Fuel 4 (1990) 221–225.
[2] M.J. Antal, M. Grønli, The art, science, and technology of charcoal production, Ind. Eng. Chem. Res. 42 (2003) 1619–1640.
[3] K. Elyounssi, J. Blin, M. Halim, High-yield charcoal production by two-step pyrolysis, J. Anal. Appl. Pyrolysis 87 (2010) 138–143.
[4] K. Elyounssi, F.-X. Collard, J.-A.N. Mateke, J. Blin, Improvement of charcoal yield by two-step pyrolysis on eucalyptus wood: a thermogravimetric study, Fuel 96 (2012) 161–167.
[5] V. Strezov, Iron ore reduction using sawdust: experimental analysis and kinetic modeling, Renew. Energy 31 (2006) 1892–1905.
[6] I. Ahmed Hared, J.-L. Dirion, S. Salvador, M. Lacroix, S. Rio, Pyrolysis of wood impregnated with phosphoric acid for the production of activated carbon: kinetics and porosity development studies, J. Anal. Appl. Pyrolysis 79 (2007) 101–105.
[7] C.J. Durán-Valle, M. Gómez-Corzo, J. Pastor-Villegas, V. Gómez-Serrano, Study of cherry stones as raw material in preparation of carbonaceous adsorbents, J. Anal. Appl. Pyrolysis 73 (2005) 59–67.
[8] D. Fabbri, C. Torri, K.A. Spokas, Analytical pyrolysis of synthetic chars derived from biomass with potential agronomic application (biochar). Relationships with impacts on microbial carbon dioxide production, J. Anal. Appl. Pyrolysis 93 (2012) 77–84.
[9] J.W. Gaskin, C. Steiner, K. Harris, K.C. Das, B. Bibens, Effect of low temperature pyrolysis conditions on biochar for agriculture use, Trans. Am. Soc. Agric. Eng. 51 (2008) 2061–2069.
[10] K. Mochidzuki, F. Soutric, K. Tadokoro, M.J. Antal, M. Tóth, B. Zelei, et al., Electrical and physical properties of carbonized charcoals, Ind. Eng. Chem. Res. 42 (2003) 5140–5151.
[11] A. Celzard, J.F. Marêché, F. Payot, G. Furdin, Electrical conductivity of carbonaceous powders, Carbon 40 (2002) 2801–2815.
[12] O. Paris, C. Zollfrank, G.A. Zickler, Decomposition and carbonisation of wood biopolymers—a microstructural study of softwood pyrolysis, Carbon 43 (2005) 53–66.
[13] A.K. Kercher, D.C. Nagle, Microstructural evolution during charcoal carbonization by X-ray diffraction analysis, Carbon 41 (2003) 15–27.
[14] J. Rodriguez-Mirasol, T. Cordero, J.J. Rodriguez, High temperature carbons from kraft lignin, Carbon 34 (1996) 43–52.
[15] P. Tingaut, Modification de la structure chimique du bois par des alcoxysilanes diversement substitués (Ph.D. thesis), University Bordeaux 1, France, 2006.
[16] J.I. Morán, V.A. Alvarez, V.P. Cyras, A. Vázquez, Extraction of cellulose and preparation of nanocellulose from sisal fibers, Cellulose 15 (2008) 149–159.
[17] M. Fan, D. Dai, B. Huang, Fourier transform infrared spectroscopy for natural fibres, in: S. Salih (Ed.), Fourier Transform – Materials Analysis, New York, InTech, 2012, pp. 45–68.
[18] M. Keiluweit, P.S. Nico, M.G. Johnson, M. Kleber, Dynamic molecular structure of plant biomass-derived black carbon (biochar), Environ. Sci. Technol. 44 (2010) 1247–1253.
[19] D.-A.Z. Wever, H.J. Heeres, A.A. Broekhuis, Characterization of Physic nut (*Jatropha curcas* L.) shells, Biomass Bioenergy 37 (2012) 177–187.
[20] Z. Wang, J. Cao, J. Wang, Pyrolytic characteristics of pine wood in a slowly heating and gas sweeping fixed-bed reactor, J. Anal. Appl. Pyrolysis 84 (2009) 179–184.
[21] J. Pastor-Villegas, J.M. Meneses Rodríguez, J.F. Pastor-Valle, M. García García, Changes in commercial wood charcoals by thermal treatments, J. Anal. Appl. Pyrolysis 80 (2007) 507–514.
[22] G. Cheng, P. Varanasi, C. Li, H. Liu, Y.B. Melnichenko, B.A. Simmons, et al., Transition of cellulose crystalline structure and surface morphology of biomass as a

function of ionic liquid pretreatment and its relation to enzymatic hydrolysis, Biomacromolecules 12 (2011) 933–941.

[23] J. Bourke, M. Manley-Harris, C. Fushimi, K. Dowaki, T. Nunoura, M.J. Antal, Do all carbonized charcoals have the same chemical structure? 2. A model of the chemical structure of carbonized charcoal, Ind. Eng. Chem. Res. 46 (2007) 5954–5967.

[24] A.J. Smith, M.J. MacDonald, L.D. Ellis, M.N. Obrovac, J.R. Dahn, A small angle X-ray scattering and electrochemical study of the decomposition of wood during pyrolysis, Carbon 50 (2012) 3717–3723.

[25] F. Kurosaki, K. Ishimaru, T. Hata, P. Bronsveld, E. Kobayashi, Y. Imamura, Microstructure of wood charcoal prepared by flash heating, Carbon 41 (2003) 3057–3062.

[26] B. Brandt, C. Zollfrank, O. Franke, J. Fromm, M. Göken, K. Durst, Micromechanics and ultrastructure of pyrolysed softwood cell walls, Acta. Biomater. 6 (2010) 4345–4351.

[27] Y. Yu, B. Fei, B. Zhang, X. Yu, Cell-wall mechanical properties of bamboo investigated by in-situ imaging nanoindentation, Wood Fiber Sci. 39 (2007) 527–535.